Groundwater Feedbacks on Climate Change in the CNRM Global Climate Model

Jeanne Colin, Bertrand Decharme, Julien Cattiaux, David Saint-Martin

Groundwater feedbacks on climate change in the CNRM global climate model

Jeanne Colin[a], Bertrand Decharme[a], Julien Cattiaux[a] & David Saint-Martin[a]

[a] *CNRM, Météo-France, CNRS, Toulouse, France*

Corresponding author : Jeanne Colin, jeanne.colin@meteo.fr

ABSTRACT

Groundwater and climate interact in a two-way manner. Precipitation ultimately controls groundwater recharge and conversely, groundwater may influence climate through evapotranspiration. Yet, very few global climate models or Earth system models actually simulate groundwater flows. And while the expected impacts of climate change on groundwater resources are the subject of a growing concern, global scale groundwater-climate feedbacks have received very little attention so far.

Here we show that the integration of unconfined aquifers in a global climate model can regionally affect the climate change signal on temperatures and precipitation. We assess the impact of groundwater under pre-industrial and $4xCO_2$ conditions (after climate stabilization). In both cases, we find that groundwater has a cooling and a wetting effect in certain regions of the world. In Eastern Europe, both these impacts are stronger in the warmer climate ($4xCO_2$ forcing) where the presence of groundwater reduces the frequency of summer heatwaves by 40%, compared to a 15% reduction in the pre-industrial world.

This work constitutes one of the very first global assessment of the potential feedbacks of groundwater on climate change. Our results support the idea that groundwater should be represented in global climate models and Earth system models, as it does indeed play an active role in the climate system.

1. Introduction

In many parts of the world, soil water can be separated into two hydrological layers: (1) the vadose zone (unsaturated soil) which is located between the surface and the water table and which holds soil moisture; (2) the saturated zone, lying underneath, which is composed of aquifers with 3-dimensional groundwater flows. Most global climate models and Earth system models do not represent groundwater flows. They only simulate the vertical transport of soil moisture in the vadose zone. In doing so, they may be neglecting an additional source of water for the atmosphere.

Groundwater was recently estimated to provide 23% of the water transpired by plants at the global scale (Evaristo and McDonnell 2017). This figure accounts for all the regions/seasons where groundwater is accessible to the vegetation root system. But this does not mean that adding groundwater in a global climate model should increase by as much the

simulated global transpiration. Where and whenever the model simulates enough soil moisture to meet the evaporative demand in the absence of groundwater, adding groundwater will not increase transpiration – even when in reality, part of the water transpired does indeed come from the underlying aquifer. In other words, the lack of groundwater representation in a model is likely to induce an underestimation of transpiration only where and when groundwater is available to plants whose transpiration is limited by the lack of soil moisture in the vadose zone. These situations correspond to "water-limited regimes" of evapotranspiration (Seneviratne et al. 2010) where the variations of soil moisture control those of evapotranspiration. These regimes typically occur in semi-arid environments or during the evaporation season in regions of transition between wet and arid climates (Koster et al. 2006; Dirmeyer et al. 2009; Dirmeyer 2011). Under such conditions, a soil moisture-controlled increase of evapotranpiration leads to a humidification and a cooling of the near surface atmosphere (Koster et al. 2006; Seneviratne et al. 2010) which can affect temperature and precipitation mean values (Koster et al. 2006; Dirmeyer et al. 2009; Seneviratne et al. 2010) and extremes (Fischer et al. 2007; Hirschi et al. 2011; Miralles et al. 2014). Therefore, to the extent that some aquifers are shallow enough to contribute to evapotranspiration where it is water-limited, groundwater may have a significant influence on the climate system.

Shallow aquifers are generally found under wet climates where soil moisture tends to be plentiful. However, drier environments can also sustain relatively shallow water table depths. This can happen in areas of complex terrain, with a convergence of the lateral groundwater flows in valleys, or in regions characterized by a pronounced seasonal cycle of precipitation, where the groundwater recharge occurring in the rainy season maintains the aquifer at a relatively high level during the dry season (Fan 2015) allowing plants to access groundwater in the capillary fringe of the vadose zone (Fan et al. 2019).

Over the last two decades, models simulating groundwater have been coupled to land surface and atmospheric models over limited-area domains, ranging in size from the watershed to the regional scale. This body of literature has shown that taking groundwater into account can indeed increase soil moisture and evapotranspiration, which can affect the boundary layer height and stability (Maxwell et al. 2007; Larsen et al. 2016; Forrester and Maxwell 2020), as well as mean precipitation (Anyah et al. 2008 ; Jiang et al. 2009; Leung et al. 2011; Larsen et al. 2016) and temperature (Anyah et al. 2008 ; Jiang et al. 2009), and possibly heat waves (Keune et al. 2016; Mu et al. 2022; Furusho-Percot et al. 2022). However, relatively few of these studies (Leung et al. 2011; Larsen et al. 2016; Keune et al.

2016; Furusho-Percot et al. 2022) used simulations which were long enough to provide climate-relevant results. And all of them were conducted with limited-area models over domains located in the United States of American, Europe or Australia, thus failing to provide a global picture.

The possible effects of groundwater on climate have recently started to be studied at the global scale with global climate models using idealized configurations (Wang et al. 2018) or schematized representations of groundwater flows (Arboleda et al. 2022). These first results indicate that even at the relatively low resolutions of global climate models, the inclusion of a groundwater scheme can indeed affect the simulated climate conditions and also modulate the regional patterns of the climate change signal (Arboleda et al. 2022) as previous studied had indirectly suggested (Maxwell and Kollet 2010; Fergusson and Maxwell 2010).

In the present study, we pursue this effort of globally assessing of groundwater-climate feedbacks in a changing climate. To this end, we use the CNRM-CM6-1 global climate model (Voldoire et al. 2019; Roehrig et al. 2020) and its process-based hydrogeological parameterization of unconfined aquifers (Vergnes et al. 2012; Vergnes et al. 2014; Decharme et al. 2019). We compare simulations performed with and without groundwater, under pre-industrial levels of atmospheric CO_2 and after climate stabilization following an abrupt quadrupling of these pre-industrial levels of CO_2 ($4xCO_2$).

The model and experimental setup are described in detail in section 2. Results are presented in section 3. First, we analyze the effect groundwater on soil moisture and evaluate the realism of the groundwater contribution to evapotranspiration in CNRM-CM6-1 under pre-industrial conditions. Then, we show the regional impacts of groundwater on climate change, starting with the impacts of groundwater in the stationary climate of the pre-industrial world. We also explain the physical processes involved in the groundwater-climate feedbacks and their evolution with climate change. Finally, in section 4, we give the main conclusions and discuss the possible underestimation of groundwater-climate feedbacks in our simulations.

2. Methods

a. Model

CNRM-CM6-1 (Voldoire et al. 2019) is the global climate model (http://www.umr-cnrm.fr/cmip6/spip.php?article11) developed in our institute (CNRM: Centre National de

Recherches Météorologiques). The simulations used in the present study were run in an atmosphere-only mode – i.e. not coupled to the ocean model.

The configuration we used is based on the ARPEGE-Climat v6.3 atmospheric general circulation model (Roehrig et al. 2020) and the SURFEX v8.0 surface modeling platform which includes the land surface model ISBA (Interaction Soil-Biosphere-Atmosphere) coupled to the CTRIP (CNRM version of the Total Runoff Integrating Pathways) river routing model (Decharme et al. 2019) (http://www.umr-cnrm.fr/spip.php?article1092&lang=en). A complete description and validation of the surface and atmospheric models can be found in the cited reference papers. Here, we only remind the main features.

The horizontal resolution is about 1.4° at the equator for ARPEGE-Climat and ISBA, and 0.5° for CTRIP. There are 91 vertical levels up to 0.01 hPa in the atmosphere, 14 soil levels down to 12 m and 12 snow levels. At the land surface, a plant-climate interactive scheme (Delire et al. 2020) controls the vegetation transpiration and growth (prognostic Leaf Area Index – LAI). There are 16 different vegetation types and 3 non-vegetation surface types in ISBA, clustered in 12 different surface tiles in the version used in CNRM-CM6-1, each with a different set of parameters, among which are the rooting depth and the vertical root density profiles.

In the soil, the evolution of the temperature and the water content are computed with an explicit diffusion scheme using the one-dimensional Fourier and Darcy laws and accounting for the hydraulic and thermal properties of the soil organic carbon. The use of a multilayer snow model of intermediate complexity allows to separate the water and energy budgets in the soil and the snowpack. CTRIP simulates the river flow, inundation dynamics and groundwater flow.

The CNRM-CM6-1configuration we used is almost identical to the one used for the CMIP6 (Coupled Models Intercomparison Project Phase 6) (Eyring et al. 2016) experiments, except for the activation of the interactive LAI scheme (which was turned off in the CNRM-CM6-1 CMIP6 experiments) and a slight modification in the groundwater scheme (see next paragraph).

b. Groundwater representation

CNRM-CM6-1 represents unconfined aquifer processes in the world's major groundwater basins at a 0.5° resolution. The hydrogeological modeling of groundwater dynamics is based on the well-known MODCOU hydrogeological model (Ledoux et al. 1989). It consists in a

one-layer diffusive 2D scheme (embedded in CTRIP) which computes the piezometric head as a function of the lateral groundwater flow, the two-way water exchange with the river (also computed in CTRIP) and the two-way vertical water exchange with the unsatured soil column of the vadose zone (represented in ISBA), as detailed in Vergnes et al. (2014) and Decharme et al. (2019).

Groundwater basins boundaries were defined using the following global maps: the Worldwide Hydrogeological Mapping and Assessment Programme (WHYMAP), the hydrogeological map over the United States from the U.S. Geological Survey (USGS) and the global map of lithology (Dürr et al. 2005). The latter was also used to determine the transmissivity and the effective porosity coefficent in each basin. In each grid cell, the Water Table Depth (WTD) accounts for the 1-km resolution topography which is extracted from the Global Multi-resolution Terrain Elevation Data 2010 (Danielson and Gesch, 2011). WTD is computed in relation to the mean elevation of the 1-km subgrid points located below the first decile of the subgrid topography (instead of the mean elevation of the grid cell). That way, WTD is representative of the "low-land" part of the grid cell, whose elevation is close to that of the river. Consequently, the upward capillary flux into the ISBA soil column is allowed only over a fraction f_{wtd} which corresponds to the area over which the water table head is close to the surface. f_{wtd} is computed dynamically as a function of the river bed elevation and the "subgrid" water table depth (computed as the depth of the water table head at a resolution of 1-km, using the subgrid topography) (Vergnes et al. 2014). Over this f_{wtd} fraction of the grid cell, the water flux between the aquifer and the soil column is bidirectional (downward recharge from the soil to the aquifer and upward capillary rise from the aquifer to the soil column). Over the rest of the grid cell (1-f_{wtd}), this water flux only represents the downward recharge of groundwater (see Annex A for further details). Given that the water table depth is representative of the "low land" part of the grid cell, it would be unrealistic to simulate capillary rise over the whole grid cell. This feature can also be seen as a way to account for the subgrid hillslope groundwater flow.

The modeling of groundwater and other hydrological processes in ISBA-CTRIP has been thoroughy validated in previous publications, both at the regional and global scales, in offline (Decharme et al. 2019; Vergnes et al., 2012; Vergnes and Decharme 2012; Vergnes et al. 2014; Munier and Decharme 2022) and inline configurations (Voldoire et al. 2019; Roehrig et al. 2020). Model results were compared to in-situ data of piezometric head, large datasets of river discharge observations and GRACE terrestrial water storage estimates. The water

table depths were also compared to the global data set of Fan et al. (2013) derived from a high-resolution groundwater model constrained with observations (Decharme et al. 2019). The ISBA-CTRIP land surface system was then used in a number of studies dealing with global hydrology and/or climate change (Ardilouze et al. 2019; Giffard et al. 2019; Douville et al. 2020; Padron et al. 2020; Pellet et al. 2020; Saint-Martin et al. 2021).

In the version of the groundwater parameterization we used here, the coupling between the saturated zone (groundwater in CTRIP) and the vadose zone (soil column in ISBA) was slightly improved compared to the formulation described in the reference papers (Vergnes et al. 2014; Decharme et al. 2019). In the latter, the water table is considered to be below the vadose zone for the coupling, even when the water table depth computed by CTRIP is shallower than the vadose zone depth in ISBA. The coupling formulation was improved to allow the water table to actually penetrate the vadose zone. The corresponding equations are detailed in Appendix A. This improvement has a minor impact on water table depths, which was evaluated both in offline and inline configurations (not shown).

In ISBA-CTRIP, plant rooting depth only depends on the vegetation type, regardless of the typical range of water table depth in a given environment. Studies have shown that in reality, plants adapt their rooting depth to the local profile of soil water availability. If the water table remains shallow throughout the year, roots also stay shallow to avoid anoxia in the saturated zone. In drier environments, plants can send deep roots in the capillary fringe to sustain their water demand (Fan et al. 2017, 2019). Therefore, having a fixed rooting depth for each vegetation type is somewhat unrealistic. The way it may affect our results regarding the impact of groundwater in our model will be discussed in sections 3.a and 4.

c. Experimental setup

We performed two pairs of simulations, with and without aquifers : one was carried out with pre-industrial (PI) levels of atmospheric CO_2 concentration, and the other with a quadrupling of the pre-industrial CO_2 concentration ($4xCO_2$). The simulations with aquifers were performed using the groundwater parameterization described in the previous paragraph (that is, with 2D groundwater flows, 2-way water exchanges with the river and the unsaturated soil column). The simulations without aquifers have no representation whatsoever of groundwater ; the water drained at the bottom of the unsaturated soil column is directly transported to the river. In the following, **PIa** (**C4a**) refers to the simulation with

aquifers under pre-industrial ($4xCO_2$) conditions, and **PIr** (**C4r**) is the reference simulation without aquifers.

All simulations were run in a stand-alone configuration (i.e. not coupled to the ocean). The model was forced with monthly climatologies of sea surface temperature and sea ice cover derived from the corresponding fully coupled simulations which were performed with CNRM-CM6-1 for CMIP6 (namely, the piControl and the abrupt-$4xCO_2$ simulations). The sea surface temperature and sea ice cover climatologies were built with the same procedure as the one used to run all atmosphere stand-alone simulations in CMIP6 (Taylor et al. 2000).

The initialization was done using restart files extracted from the piControl and abrupt-$4xCO_2$ CMIP6 simulations run with CNRM-CM6-1. We used the restart files of the year 1850 of the piControl simulation for **PIr** and **PIa**, and those of the 150th year of the abrupt-$4xCO_2$ simulation for **C4r** and **C4a** so that the model has reached its equilibrium state in both cases.

As the interactive plant-climate scheme was not activated in CNRM-CM6-1, we extracted the Leaf Area Index and plant carbon variables values from the restart files of the CNRM-ESM2-1 (Séférian et al. 2019) CMIP6 simulations. CNRM-ESM2-1 is the Earth System Model version of CNRM-CM6-1 (http://www.umr-cnrm.fr/cmip6/spip.php?article10). In addition to the processes represented by CNRM-CM6-1, it simulates the global carbon cycle which requires the use of additional components and paramaterizations, such as the interactive plant-climate scheme.

After the initialization, a 40-year spinup was run for each simulation to ensure that all variables have adjusted to each other in the newly defined settings (that is, without aquifers, with forced SST and SIC and with the plant-climate interactive scheme). Then, all four simulations (**PIr, PIa, C4r** and **C4a**) were run for 90 years.

d. Statistical significance computations

For all significant tests performed on field differences, we used a False Detection Rate (FDR) test described by Wilks (2016). It is based on local t-tests for the computation of P-values. To determine the statistical significance of the differences over each grid points, P-values are compared to a threshold which depends on the P-values of the other grid points, the number of grid points, and the "level of confidence" of the test (in our case, 95%). This method allows to reduce the rate of false significance, which can be quite high in the case of

auto-correlated fields when P-values are directly compared to a fixed threshold corresponding the level of confidence of the test (Wilks, 2016).

For the tests performed on the 2-meter temperature fields, the ocean grid points were excluded for the computation of the threshold. As the simulations are forced by the same sea surface temperatures whether or not the groundwater scheme is activated, there are very little difference on the 2-meter temperatures over the ocean in **PIa** (respectively **C4a**) compared to **PIr** (**C4r**). Therefore, when testing the significance of the temperature differences, the P-values over ocean grid points are very close to zero, and this falsifies the computation of the significance threshold.

3. Results

a. Contribution of groundwater to soil moisture and transpiration under pre-industrial conditions

As mentioned in section 2, the CNRM-CM6-1 groundwater scheme has been thoroughly validated in previous publications. Our purpose here is not to go over this validation again. In this subsection, we analyze the effects of groundwater on soil moisture and evaluate the order of magnitude of the groundwater contribution to the global transpiration flux under pre-industrial conditions (**PI** simulations).

Fig 1.a shows that aquifers present a rather shallow water table over a large portion of the land surface **PIa** (see Fig. B1 for the seasonal variations). As explained in section 2.b, this water table depth is only representative of the "low land" part of each grid cell, whose fraction is given by f_{wtd} (Fig. 1.b and B1). f_{wtd} is larger over flat regions and when the WTD is shallow. The presence of groundwater significantly affects the root zone water content only if the water table is not much deeper than the plants rooting depth (less than ~1.5 meters) (Fig. 1.c, d and B1).

In some regions, the mean water table is shallower than the rooting depth, whereas in reality, roots do not grow in the saturated zone. On average over these regions, we find that 34% of the total root zone liquid water content is located below WTD. But deep roots have a low density, layers located below WTD only contributes to 2.2% of the total amount of water available to transpiration over these regions (the water available to transpiration is computed as the liquid water content weighted by the vertical profile of root density). Fig. B2 shows this ratio of water availability below WTD for each grid cell. On average over the regions

where WTD lies above the rooting depth, this ratio is equal 1%. So the unrealistic presence of roots located WTD in our model does not lead to a notable overestimation of transpiration in our model. It also has a very limited impact on the increase of transpiration due to the presence of groundwater. As shown on Fig B2, most of the increase of vegetation water availability in **PIa**, compared to **PIr**, involves soil layers located above the water table (98% on global average and 96.5% on average over the regions where WTD is shallower than the rooting depth). This means that the presence of shallow aquifers increases soil moisture mostly through the combined effect of capillary rise and a reduction of drainage efficiency.

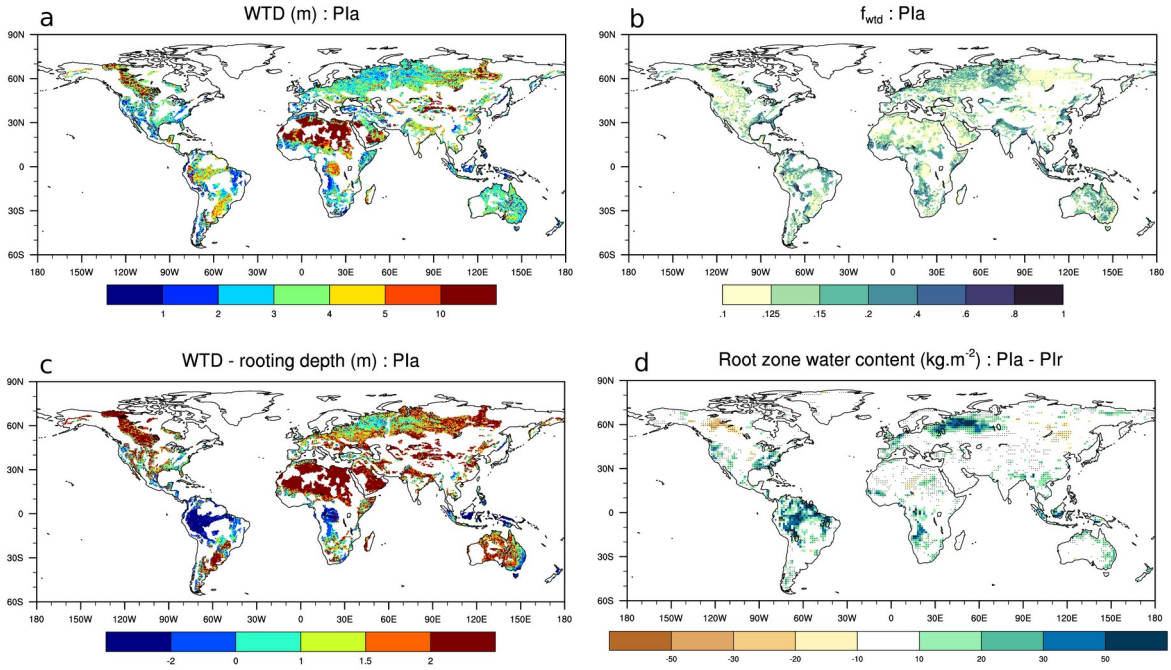

FIG. 1.

(a): mean annual Water Table Depth (WTD) in PIa ; (b): mean annual fraction of the grid cells over which capillary rise are allowed f_{wtd} ; (c): difference between the mean annual WTD and the vegetation rooting depth ; (d): mean annual root zone water content difference with and without groundwater (PIa – PIr). These fields present very limited seasonal variations (see FIG. B1).

We now consider the realism of the groundwater contribution to global transpiration simulated by CNRM-CM-6-1 under pre-industrial conditions.The validations presented in previous publications offered an indirect validation of the evapotranspiration simulated in the presence of groundwater, as the adding of groundwater improved river discharge and terrestrial water storage annual cycles (Vergnes et al. 2012; Vergnes and Decharme 2012). However, the increase of evapotranspiration induced by the presence of groundwater falls

within the range of uncertainties of these gridded estimates (Decharme et al. 2019), which makes it difficult to assess the realism of the groundwater impact on evapotranspiration at the global scale.

In a recent meta-analysis study of in situ data using water isotopes, groundwater was estimated to represent 23% of the global transpiration flux (Evaristo and McDonnell 2017). But as mentioned in section 1, this figure can not be compared to the global increase of transpiration obtained with the activation of a groundwater scheme in a global climate model (+2% over the whole land surface and +8% above the large groundwater basins represented in CNRM-CM6-1). Indeed, when transpiration is not limited by soil moisture, shallow aquifers may still provide water to the vegetation and thus contribute to the transpiration fluxes in the observed data, but this situation will not result in an increase of transpiration when comparing simulations run with and without groundwater. If there is enough soil moisture to meet the evaporative demand in the first place, the addition of groundwater will not lead to an increase of transpiration. We can however derive an upper estimate of the proportion of groundwater transpired by groundwater-dependent ecosystems, $\boldsymbol{T_{gw}}$, in **PIa**, the pre-industrial simulation with aquifers (where the simulated climate is fairly close to the present-day one) and compare it with the results of another meta-analysis study of in situ data (Barbeta and Peňuelas 2017) which concluded that groundwater accounts for 38% of the global transpiration flux of groundwater-dependent ecosystems (instead of all ecosystems).

To do so, we only consider the grid points over which the annual averaged transpiration T (kg.m^2.s^{-1}) is significantly modified by the presence of groundwater and we compute $\boldsymbol{T_{gw}}$ as follows:

$$T_{gw} = \frac{\sum_{i=1}^{N} \left[T_{PIa}(i) - T_{PIr}(i) \right]}{\sum_{i=1}^{N} f_{wtd}(i) T_{PIa}(i)} \quad (1)$$

where T_{PIa} (kg.m^2.s^{-1}) is the mean annual transpiration in **PIa,** T_{PIr} (kg.m^2.s^{-1}) the mean annual transpiration in **PIr,** the reference simulation without aquifers, f_{wtd} is the fraction over which the capillary rise is allowed and i the indexes of the N grid points over which (T_{PIa} - T_{PI}) is statistically significant at the 95%-level confidence.

For each of the N grid points where the presence of groundwater affects the mean annual transpiration flux, $(T_{PIa}(i) - T_{PIr}(i))$ represents the increase of transpiration due to the inclusion of groundwater – it is always positive. $f_{wtd}(i) T_{PIa}(i)$ corresponds to the transpiration

flux over the fraction of the grid cell over which the vegetation can be considered groundwater-dependent. We find T_{gw} is equal to 34%. If the increase of transpiration in **PIa** solely stemmed from groundwater, T_{gw} would represent the relative contribution of groundwater to transpiration flux for groundwater-dependent ecosystems in our model. But as previously mentioned, the increase of water available to transpiration in PIa is not only due to capillary rise from the aquifer but also to a less efficient drainage of soil moisture above shallow aquifers. Our modeling framework does not allow to disentangle these two effects in order to quantify the actual contribution of groundwater in the increase of water availability. We can only state that groundwater contributes to part of the additional transpiration in **PIa**, making T_{gw} an upper estimate of the contribution of groundwater to transpiration. The value of T_{gw} being slightly lower than the 38% found by Barbeta and Peňuelas (2017), the contribution of groundwater to transpiration in groundwater-dependent environments is thus likely to be underestimated in our model. They may be due to the lack of dynamical rooting depth in ISBA which could limit the uptake.

b. Groundwater impacts on climate under pre-industrial conditions

Before we assess the impacts of the presence groundwater on the climate change signal between the Pre-industrial and 4xCO_2 simulations, we explore the impact of groundwater on a stationary climate by comparing the **PIa** and **PIr** simulations (with and without aquifers).As explained in introduction, a shallow water table depth is not sufficient to enhance evapotranspiration. For this to happen, a number of conditions has to be met. As shown in the previous subsection, the water table depth must not be much deeper than the plant rooting depth to affect the root zone water content. Then, for the increase of soil water content to translate into an increase of vegetation water availability, the soil must neither be frozen (as in northwestern Russia in winter and spring) nor already close to the field capacity (as in Indonesia) and the increase of water content must not affect only deep soil layers with a low root density (as in Amazonia) (Fig. 2). Finally, the increase of vegetation water availability must occur in water-limited regimes of evapotranspiration, which can be characterized by strong values of the cross-correlation between evapotranspiration and vegetation water availability in **PIr** (Fig. 2).

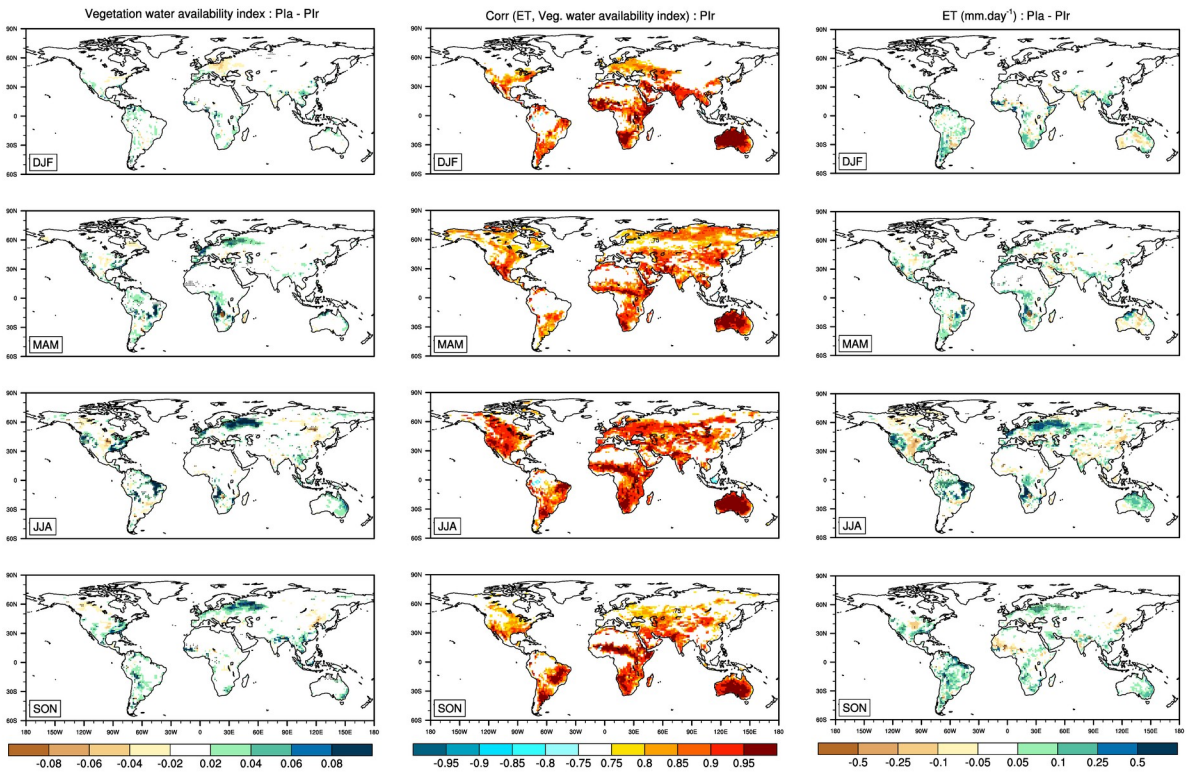

FIG. 2

Left panel: mean seasonal differences (PIa – PIr) of the vegetation water availability index (computed as the Soil Wetness Index, with a weighting of soil water content with root density along vertical layers) ; middle panel: mean seasonal cross-correlation of water stress index with evapotranspiration ; right panel: mean seasonal differences (PIa – PIr) of evapotranspiration.

In our simulations, all these conditions are predominantly met during boreal summer and fall (JJA and SON) in western and eastern United States of America, northwestern Europe, northern Australia, the western part of the Brazilian Nordeste, the plateaus of Angola and a wider area in the eastern part of the geographical Europe we will refer to as “Eastern Europe”. Results indicate that this increase of evapotranspiration reduces the daily maximum temperatures by 0.5°C to 2°C in summer (JJA) over the three later regions (Brazil, Angola and Eastern Europe) but has no statistically significant effect on precipitations (Fig. 3).

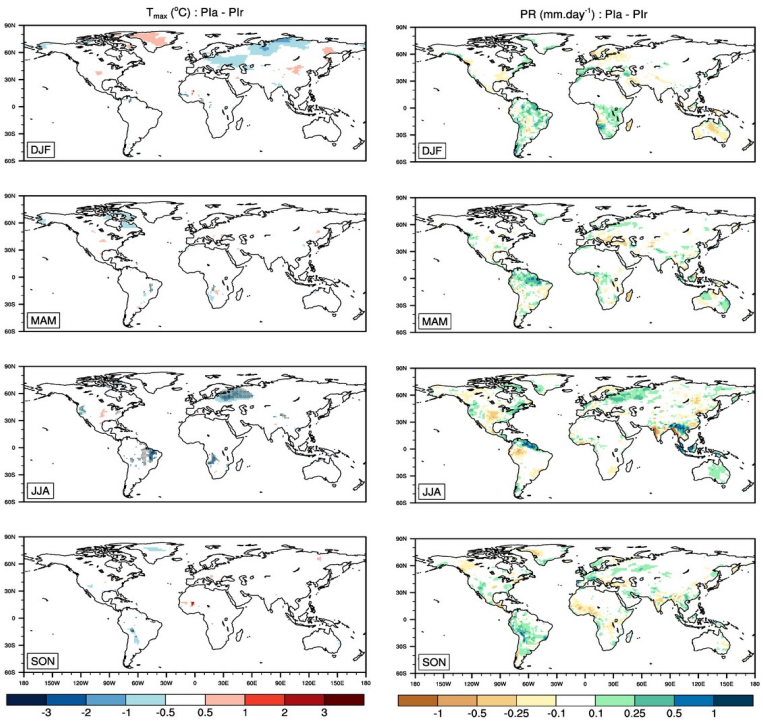

FIG. 3.

Impact of groundwater under pre-industrial conditions (**PIa** – **PIr**) on mean seasonal daily maximum 2-meter temperature (left panel) and precipitation (right panel): **PIa** – **PIr**.

c. Regional impacts of groundwater on climate change

Climate change impacts on shallow aquifers (which are the ones susceptible to impact climate in return) are significant almost everywhere (Fig. 4). They are mostly driven by precipitation changes, as the recharge rates are mainly controlled by precipitation.

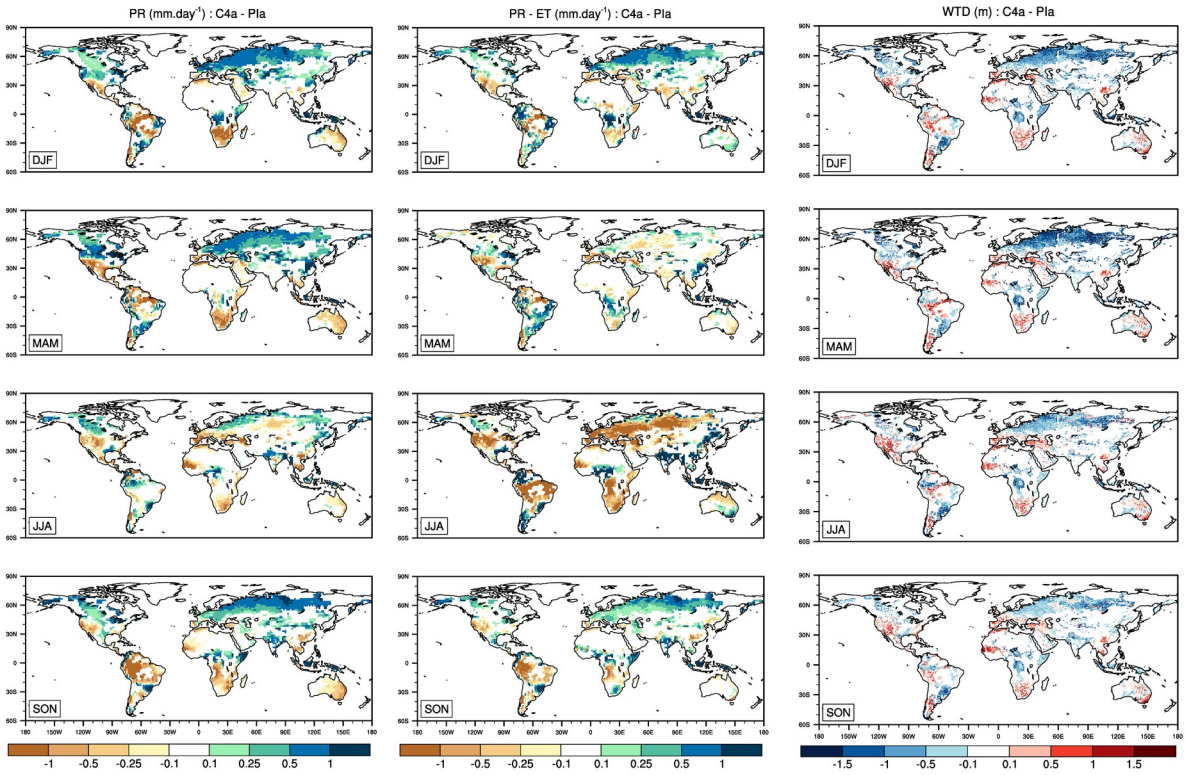

364 **FIG. 4.**

365 Climate change impact (C4a – PIa) on mean seasonal precipitation (left panel), precipitation minus
366 evapotranspiration (middle panel) and water table depth shallower than 100 meters (right panel). All
367 difference are statistically significant at a 95 % level of confidence.

368

369 In the southwestern US, Brazil Nordeste and Angola plateaus regions, the water table is
370 deeper under 4xCO_2 conditions and thus, groundwater has a smaller effect on
371 evapotranspiration. However, this does affect much the 2-meter temperature and precipitation
372 (Fig. 5).

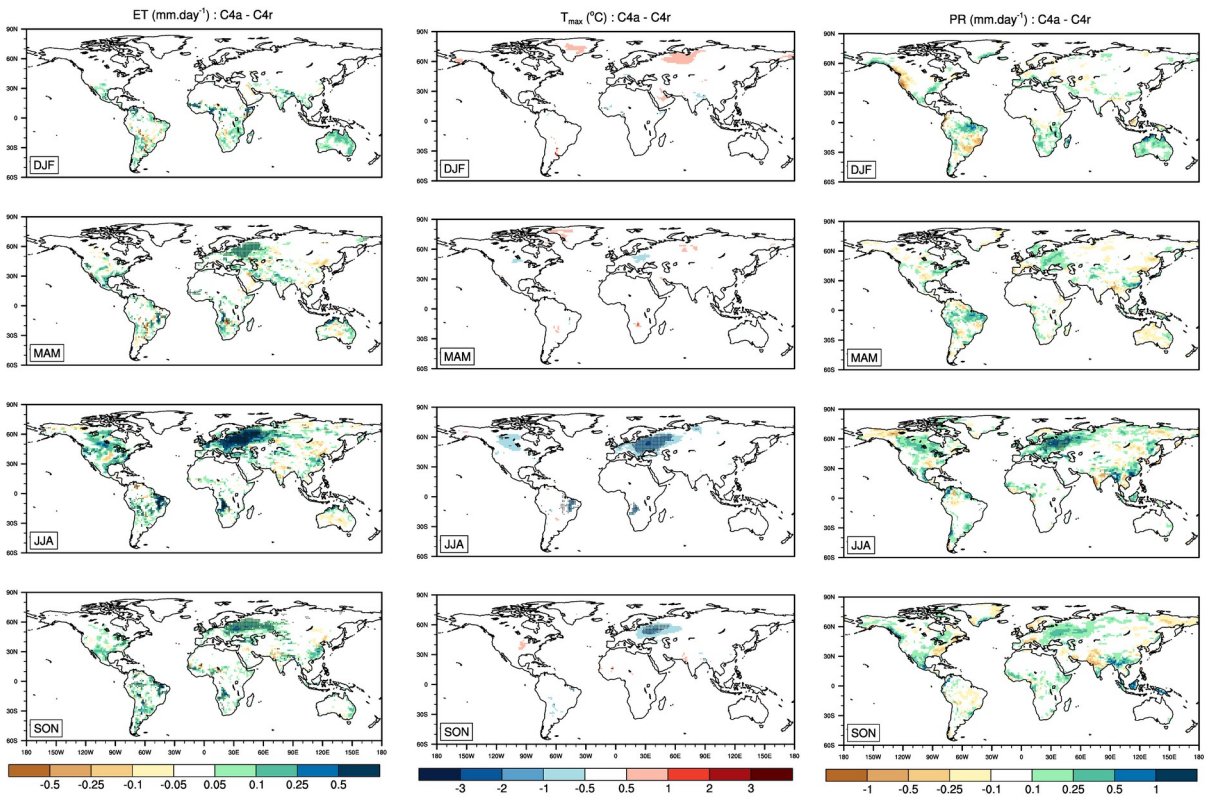

FIG. 5.

Impact of groundwater under 4xCO2 conditions (C4a – C4r) on seasonal evapotranspiration (left panel), daily maximum 2-meter temperature (middle panel) and precipitation (right panel). The stippling indicate statistically significant differences at a 95% level of confidence.

In Eastern Europe, the situation is reversed with a higher impact of groundwater on evapotranspiration under 4xCO_2 conditions. Figures 6 and 7 offer a closer look at the effects it has on temperature and precipitation during the extended boreal summer season (June to September) in Eastern Europe.

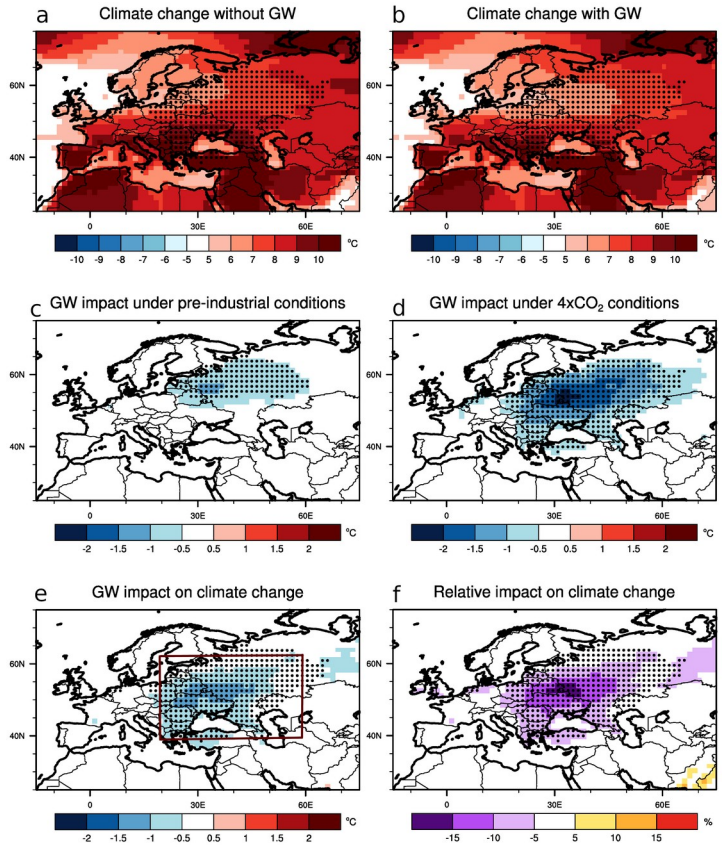

FIG. 6.

Impact of groundwater on the mean summer (JJAS) 2-meter daily maximum air temperature (°C) under pre-industrial and 4xCO_2 conditions over Europe. (a) Climate change signal without groundwater (C4r – PIr); (b) climate change signal with groundwater (C4a – PIa); (c) impact of groundwater in the pre-industrial simulations (PIa – PIr); (d) impact of groundwater in the 4xCO2 simulations (C4a – C4r); (e) impact of groundwater on the climate change signal [(d) - (c)]; (f) relative impact of groundwater on the climate change signal [100.(e)/(a)]. On (c) and (d), the stippling shows significantly statistical differences at the 95% level of confidence. On (a), (b), (e) and (f), the stippling is the one computed for (d). The rectangle on (e) shows the "Eastern Europe" box over which variables are spatially averaged for Figures 8, 10, B3 and Table 1.

In this region, the differences on the mean summer daily maximum temperatures remain below 1°C in **PIa** compared to **PIr**, but they reach 2°C in **C4a** compared to **C4r**, with a cooling zone spreading further down South (Fig. 6). In other words, there is a significant differential impact of groundwater ([**C4r - C4a**] – [**PIa – PIr**]) on maximum daily temperatures, which locally amounts to 20% of the climate change signal. If we consider the spatially averaged percentiles of daily minimum and maximum temperatures over Eastern

Europe ([19°E – 60°E / 40°N – 62°N]) (Fig. B3), we find that the cooling induced by the presence of groundwater is stronger for the warmer values of temperatures.

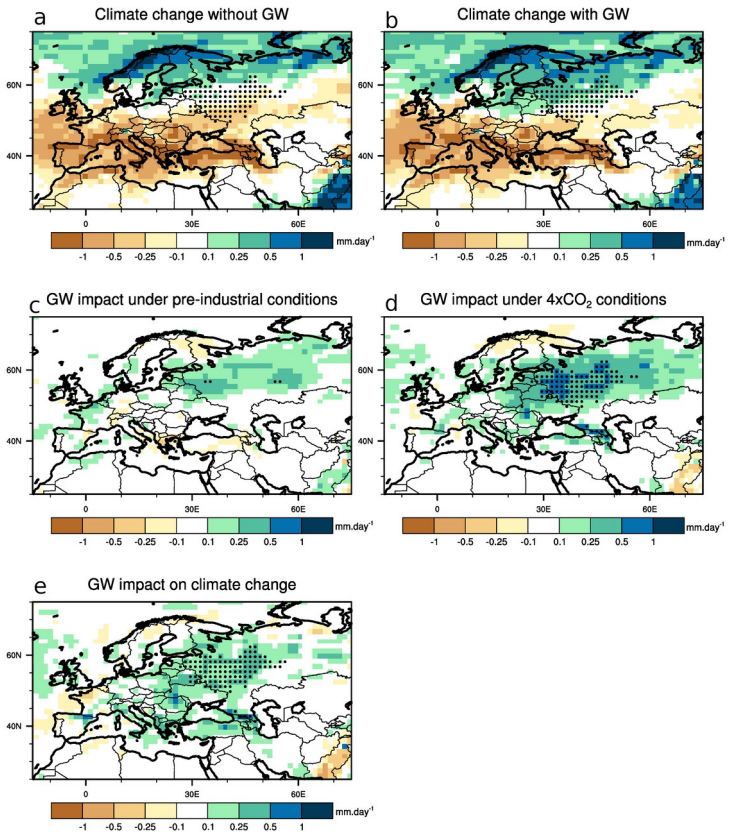

FIG. 7.

Impact of groundwater on mean precipitation (mm.day^{-1}) under pre-industrial and 4xCO2 conditions over Europe. a, b, c, d, e : Same as FIG.7 for precipitation.

The impact of groundwater on precipitation is not significant in the pre-industrial simulations, but we find an increase of summer precipitation over Eastern Europe in the warmer climate under 4xCO_2 conditions (Fig. 7). In **C4a**, the mean precipitation is 0.4 mm.day^{-1} larger (i.e. 30%) than it is in **C4r**, with a maximum relative increase centered around the median values of daily precipitation (Fig. B3). In this region, the climate change signal corresponds to a drying in the South and a wetting in the North, so the presence of aquifers leads to a southward shift of the drying/wetting limit.

To further understand the processes involved in this differential impact of groundwater, we now consider the annual cycles of the water exchanges between the atmosphere, the

vadose zone and the deep saturated zone (aquifers) in all four simulations over the Eastern Europe box (Fig. 8 and 9).

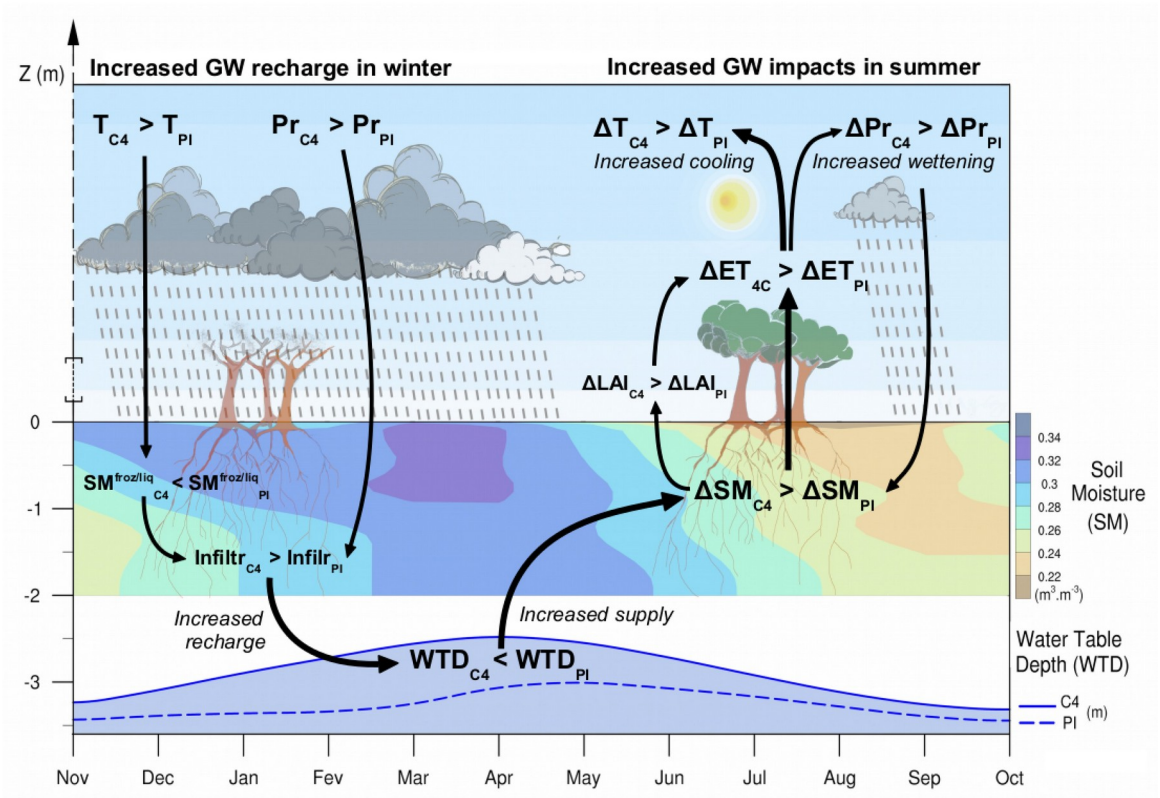

FIG. 8.

Semi-conceptual sketch of the main mechanisms involved in the groundwater-climate feedbacks in a changing climate over Eastern Europe.

The y-axis represents the depth (in meters) below the surface, and the x-axis the time of the year (in months). The seasonal variations of the Soil Moisture (SM) are shown by the coloured shading which represents the mean annual cycle of the liquid water content (m3.m-3) in the vadose zone, averaged over the Eastern Europe box in the C4a simulation. Below are the mean annual cycle of the Water Table Depth (WTD) in the pre-industrial (PI) and 4xCO2 simulations (C4). The arrows and inequalities illustrate the physical processes detailed in the main text. T refers to the air temperature, Pr the precipitation, ET the evapotranspiration, SMfroz/liq the ratio of frozen and liquid water contents in the vadose zone, Inflitr the infiltration of liquid water, and LAI the Leaf Area Index.

We find that during the groundwater recharge season (from October to April/May), the precipitation rates are much larger in **C4a** than in **PIa** (+35%). Additionally, in the warmer climate under $4xCO_2$ conditions, there is less frozen water in the vadose zone, which allows for a better infiltration of the precipitation. Indeed, in the pre-industrial climate, a larger

fraction of the winter precipitation ends up in surface runoff, either as rain falls on a frozen ground or later on, during the spring thaw. These two features are part of climate change and their amplitude does not significantly differ whether or not groundwater is represented in the model. Combined, these features result in a larger groundwater recharge and a shallower water table with the $4xCO_2$ climate forcing. As the summer progresses, the water table deepens in both **C4a** and **PIa**, and the differences between the two are reduced as more water is transferred to the vadose zone in **C4a**. The presence of groundwater thus causes a larger gain of summer soil moisture with the $4xCO_2$ climate forcing. The induced increase of evapotranspiration is subsequently amplified, leading to stronger cooling and wetting effects of groundwater under the $4xCO_2$ conditions. Finally, the increase of precipitation in **C4a** creates a positive feedback on evapotranspiration. This feedback can explain why the plant transpiration does not increase more than the bare soil evaporation does, contrary to what could be expected and has been verified in offline settings where the land surface was not coupled to the atmosphere (Maxwell and Condon 2016).

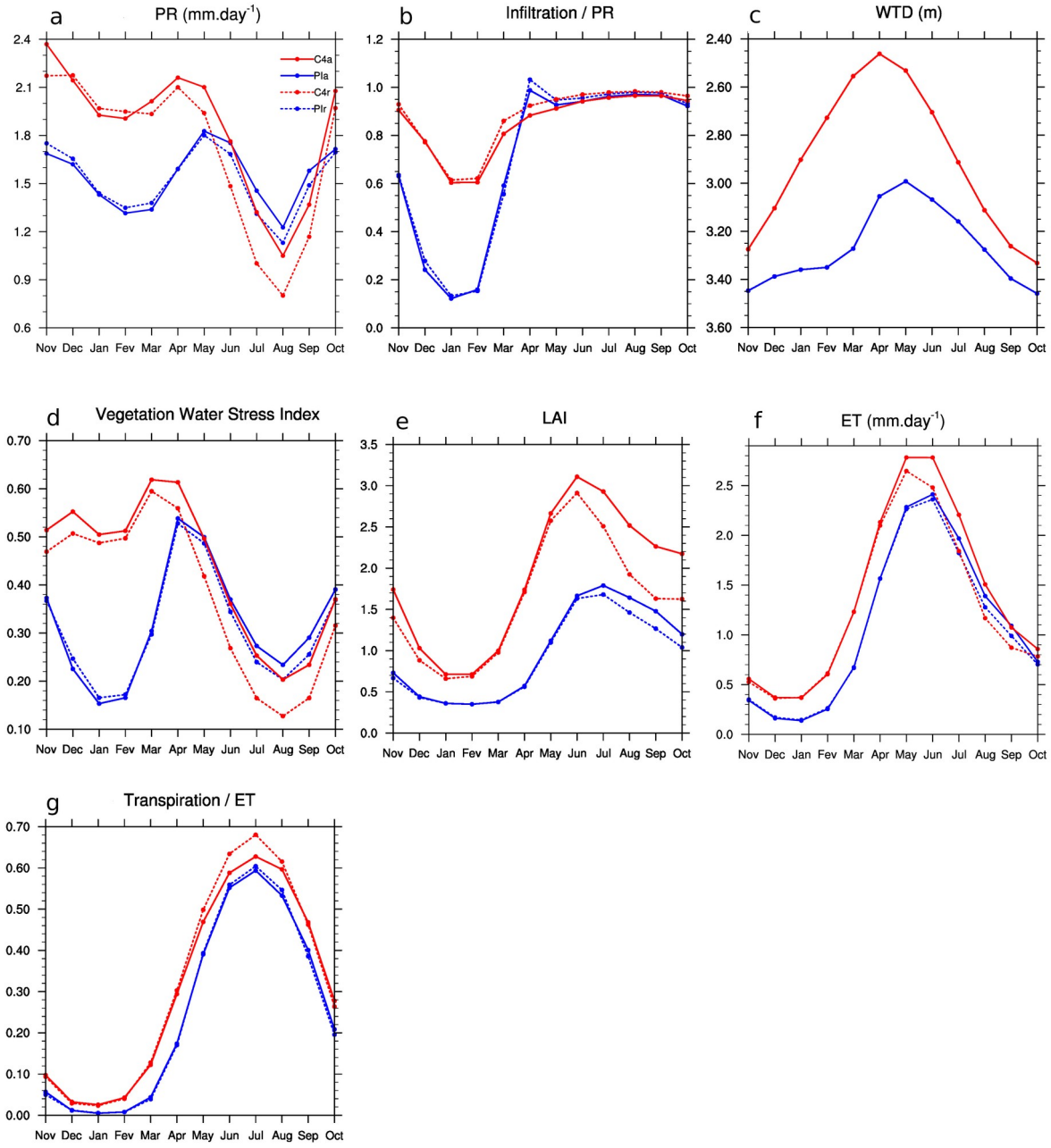

FIG. 9.

Mean annual cycles spatially averaged over the Eastern Europe box drawn on FIG. 6 (e) ([19°E – 60°E / 40°N – 62°N]) of (a) precipitation (mm.day-1), (b) infiltration divided by precipitation, (c) water table depth, (d) vegetation stress index (computed as the Soil Wetness Index (SWI) for liquid water in the root zone), (e) leaf area index, (f) evapotranspiration (mm.day-1), (f) transpiration divided by evapotranspiration, for PIa (blue solid line), PIr (blue dotted line), C4a (red solid line) and C4r (red dotted line).

d. Groundwater impacts on heat waves in Eastern Europe

As groundwater has a larger impact on the warmer maximum daily temperatures over Eastern Europe (Fig. B3), summer heat waves are likely to be affected as well, and possibly to a different extent with the pre-industrial and $4xCO_2$ climate forcings.

Heat waves are here defined as events characterized by a duration, a spatial extent and an intensity. The selection of days and grid points experiencing a heat wave is based on the exceedance of a percentile threshold computed in **PIr** (**C4r**) for the pre-industrial ($4xCO_2$) simulations: a grid cell is considered to experience a hot day when both the daily maximum and minimum temperatures exceed the 95^{th} percentile of their reference distributions. For both **PIr** and **PIa** (C4r and C4a), reference distributions are empirically estimated from Tmax and Tmin values of all JJAS days of the **PIr** (**C4r**) simulation. Then, a heat wave event is defined when at least 5% of the spatial domain (here the Eastern Europe box previously defined) experiences a hot day for at least 3 consecutive days. This minimum extent has been defined in order to get a reasonable sample of heat waves in the **PIr** and **C4r** simulations. Heat waves separated by less than 3 days are concatenated. The heat wave mean intensity is then defined as the maximum exceedance of the Tmax or Tmin criteria, averaged over the heat wave duration and all the grid points affected by the event. The heat wave severity is then defined as the product of duration, mean extent and mean intensity. The average of the severity across several heat waves is performed through the geometric mean, which is less sensitive to very high departures than the arithmetic mean. This procedure is a slightly adapted version of the procedure used in previous studies (Schoetter et al. 2015; Douville et al. 2016).

The statistical significance of changes in heat waves characteristics (duration, extent, intensity) is assessed with a bootstrap procedure: for each simulation we generate 1000 ensembles of N events randomly re-sampled among the N events of the simulation (with replacement), and then empirically estimate the 95%-level confidence interval associated with each characteristic.

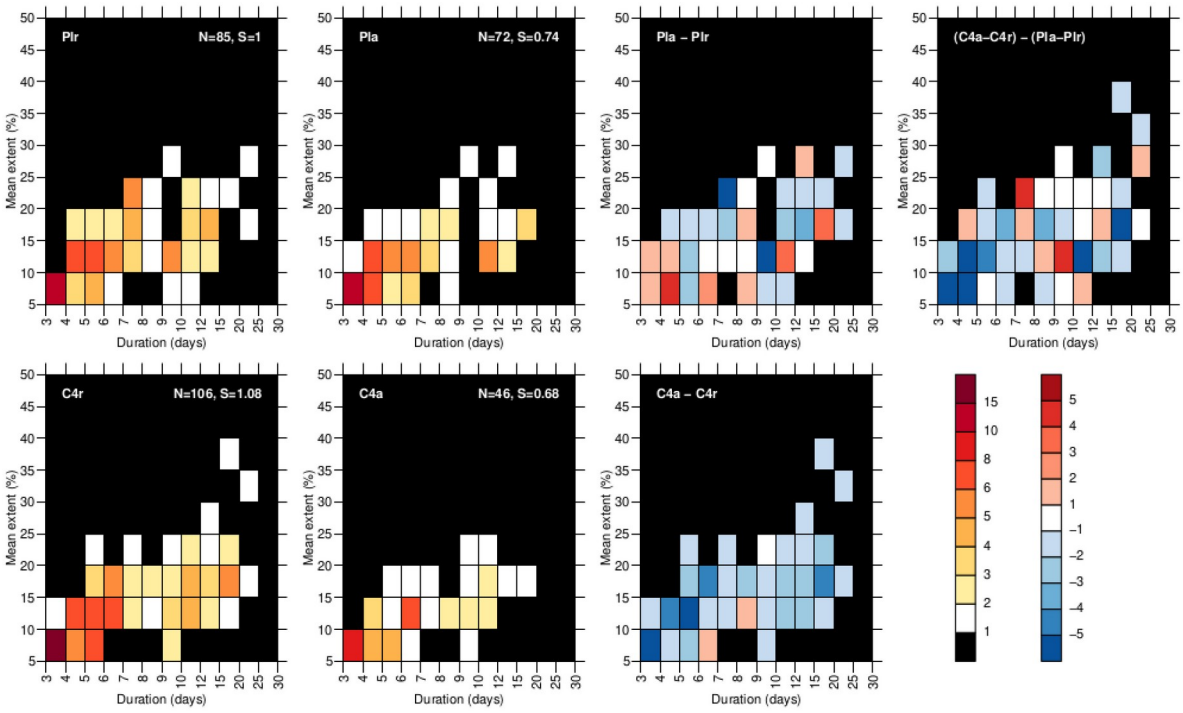

FIG. 10.

(a) to (d) Number of heat waves (HW) events per duration (in days, x-axis) and mean spatial extent (in % of the Eastern Europe box domain ([19°E – 60°E / 40°N – 62°N]), y-axis) for (a) PIr, (b) C4r, (c) PIa and (d) C4a simulations. (e) Impact of groundwater in the pre-industrial simulations [(c) – (a)]. (f) Impact of groundwater in the 4xCO2 simulations [(d) – (b)]. (g) Impact of groundwater on heat wave changes [(f) – (e)]. For (a) et (d), the total number of heat waves events (N) is indicated in the top-right corner, as well as the mean severity normalized by the PIr value (S).

FIG. 10 offers a two-dimensional view of the heat waves simulated over the Eastern Europe box, giving the number of heat wave for each duration and range of extent. It shows the effect of aquifers on heat waves is stronger in the 4xCO2 simulations. Overall, there are 57% less heat waves in C4a compared to C4r, with a decrease in the number of heat waves for almost every duration and extent. The mean duration and extent are respectively reduced by 18% and a 12% while the mean intensity remains the same, and the mean severity (defined as the product of duration, extent and intensity) is 39% weaker in C4a (Table 1). In PIa, the total number of heat waves is reduced by 15% compared to PIr, but the signal along the spectrum of durations and extents is somewhat unclear (Fig. 10), in fact none of the mean or maximum features of heat waves are significantly reduced (Table 1).

	Number	Duration	Mean Ext.	Max Ext.	Mean Int.	Max Int.	Severity
PIr	85	7.1	13.6	18.1	2.7	6.2	3
PIa	72	6.3	12.2	15.9	2.5	5.8	2.2
C4r	106	7.7	13.4	18.1	2.5	6.4	3.3
C4a	46	6.3	11.8	15.1	2.5	5.9	2

TAB. 1.

Heat waves mean and maximum characteristics in all four simulations.

It is not possible to directly assess the impact of climate change on heat waves in our simulations because nearly every summer day in the $4xCO_2$ simulations meets the criteria defining a heat wave in the pre-industrial climate. However, since the effects of groundwater on heat waves are larger under the $4xCO_2$ conditions, compared to the pre-industrial climate, one can say that groundwater has a dampening effect on the climate change-induced worsening of heat waves in Eastern Europe.

4. Discussion and conclusion

In this study, we carried out a set of 4 global climate simulations to assess the impact of groundwater on a stabilized climate, under pre-industrial and $4xCO_2$ climate forcings.

Under pre-industrial conditions, we found that the inclusion of groundwater has a limited, yet significant impact, on daily maximum 2-meter temperatures in a number of regions (Eastern Europe, parts of Brazil and southern Africa) where the presence of shallow unconfined aquifers has a cooling effect in summer, due to an increase of evapotranspiration. Then we showed that in Eastern Europe, this cooling effect of groundwater is stronger in the $4xCO_2$ simulations, thus reducing the intensity of climate change-induced warming by 5% to 20%. This differential impact of groundwater on summer temperatures translates into a reduced worsening of heat waves with climate change over this region.

We also found that while the presence of groundwater has no significant effect on precipitation in the pre-industrial simulations, it leads to an increase of summer precipitation

in Eastern Europe in the $4xCO_2$ simulations, thus affecting the climate change signal with a northward shift of the drying/wetting limit in this region.

There are good reasons to assume that if anything, the groundwater-climate feedbacks could be underestimated in our simulations. In section 3.a, we showed that the proportion of groundwater in the water transpired by plants which actually rely on aquifers was probably a little underestimated. Moreover, the fraction of this groundwater-dependent vegetation is likely to be underestimated because of the model's resolution (0.5° for groundwater) and the lack of dynamical rooting depth.

The 0.5 resolution allows for a good representation of groundwater in relatively flat regions. But when the subgrid topography is more complex, the extent of shallow water table depths is underestimated, partly by construction (see section 2.b) and partly because the lateral groundwater fluxes are weaker than they would be at a higher resolution (Krakauer et al., 2014). In CNRM-CM6-1, depending on the regions, the mean lateral groundwater flux is approximately 5 to 20 times smaller than the mean recharge flux (not shown) – locally, this ratio can drop below 1 or exceed 100. Therefore, most of the groundwater-induced increase of evapotranspiration is due to the use of the groundwater stored during the rainy season, and not to the spatial convergence of groundwater in valleys. However there are regions, like the US Rocky Mountains where the lateral flow was proven to dominate the groundwater influence on evapotranspiration (Forrester and Maxwell 2020). So the effects of groundwater may be underestimated in the regions we identified. And with a higher resolution, other regions could also turn out to be affected.

Another possible source of underestimation of the effects of groundwater lies in the fact that plant rooting depths are fixed in CNRM-CM6-1. As mentioned in section 2 and 3.a, studies have shown that to a certain extent, plants can grow deeper roots in drier environments to access an underlying groundwater resource (Fan et al. 2017, 2019). In regions where groundwater already affects climate in our simulations, the inclusion of a dynamical plant rooting depth could accentuate the increase of transpiration and the subsequent effects on air temperature and/or precipitation. The dynamical deepening of roots could also foster a groundwater/climate coupling in some of the regions where the simulated water table is currently too deep for groundwater to impact the atmosphere.

However, it is difficult to foresee how an increased resolution or a dynamical representation of plant rooting depth would affect the regional impact of groundwater on the climate change signal.

Ultimately, our study shows that even at the current resolution of global climate models and Earth system models, where the effects of groundwater may not be fully accounted for, it is worth representing aquifers, given that failing do so can regionally bias the model's response to climate change. This conclusion supports the recommendations issued by other authors in the groundwater and climate modeling communities (Clark et al. 2015; Fan et al. 2019; Gleeson et al. 2021; Arbodela et al. 2022) also calling for the inclusion of groundwater processes in Earth system models. And although the intensity and location of the groundwater impacts could vary from one model to another, the mechanism we unraveled should remain the same: wherever shallow water table depths coincide with water-limited regimes of evapotranspiration, groundwater may have a cooling and/or a wetting effect, and these effects are likely to grow stronger (weaker) in the future if mean precipitation rates increase (decrease) with climate change.

Acknowledgments.

This work was funded by Météo-France and the CNRS. The authors would like to thank the entire CNRM-CM team for their support, in particular S. Sénési for his technical assistance, and Thomas Fiolleau who created the graphic elements of Fig.3. We also thank the anonymous reviewers for their useful comments which helped improve the manuscript. We acknowledge the participants of the I-GEM project (ANR-14-CE01-0018) and the associated workshops for the fruitful discussions which helped put our work in perspective.

Data Availability Statement.

All the simulations outputs analyzed in this study are available in the Zenodo repository 10.5281/zenodo.7137879.

APPENDIX A

Groundwater-Soil coupling formulation

583 ISBA solves the evolution of soil moisture within the vadose zone using the mixed form
584 of the Richards equation for a soil discretized in N soil layers. Neglecting the soil-water
585 source/sink terms, the tendency of soil moisture in each soil layer is computed in terms of
586 volumetric water content w ($m^3.m^{-3}$), and the hydraulic gradient is computed in terms of water
587 pressure head ψ (m), as follows:

588

589 $$\frac{\partial w_i}{\partial t} = \frac{1}{\Delta z_i}\left[\left(k_i + v_i\right)\left(\frac{\psi_i - \psi_{i+1}}{z_i - z_{i+1}}\right) + k_i\right] \quad \text{(A1)}$$

590 where Δz_i (m) is the thickness of the layer i, z_i (m) is the depth of each layer mid-points or
591 nodes, and k_i ($m.s^{-1}$) and v_i ($m.s^{-1}$) are the geometric means over two consecutive nodes of the
592 soil hydraulic conductivity and isothermal vapor conductivity values (Decharme et al. 2011).
593 At the bottom of the soil column, the isothermal vapor conductivity is neglected and the soil
594 moisture is solved taking into account the soil/groundwater changes and considering that the
595 water pressure head of the water table ψ_N (m) is at saturation, as follows:

596 $$\frac{\partial w_N}{\partial t} = \frac{\left(1 - f_{wtd}\right)}{\Delta z_N} k_N + \frac{f_{wtd}}{\Delta z_N}\left[k_N\left(\frac{\psi_N - \psi_{sat}}{z_N - max\left(z_{wtd}, d_N\right)} + 1\right)\right] \quad \text{(A2)}$$

597 where f_{wtd} is the fraction of the grid cell allowing upward groundwater capillary fluxes, ψ_N
598 (m), k_N ($m.s^{-1}$) and z_N (m) are respectively the water pressure head, the hydraulic conductivity
599 and the depth of the last hydrological node N, z_{wtd} (m) is the depth of the water table, and d_N
600 (m) is the depth of the root zone which varies from 0.2 to 8 meters depending on the
601 vegetation type (Decharme et al. 2019).

602 The main limitation of this coupling formulation is that it considers the water table to be
603 lower or equal to the depth of the vadose zone in ISBA. To solve this problem, the mixed
604 form of the Richards equation (equation A1) was modified as follows:

605 $$\frac{\partial w_i}{\partial t} = \frac{\left(1 - f_{wtd}\right)}{\Delta z_i}\left[\left(k_i + v_i\right)\left(\frac{\psi_i - \psi_{i+1}}{z_i - z_{i+1}}\right) + k_i\right] + \frac{f_{wtd}}{\Delta z_i}\left[\left(k_i + v_i\right)\left(\frac{\psi_i - \psi^*_{i+1}}{z_i - z_{i+1}}\right) + k_i\right] \quad \text{(A3)}$$

606 whereψ^*_{i+1}(m) is the water potential at the equilibrium with the water table if the water table is
607 present in the soil.

608 Because the variation of water potential with depth is linear, ψ^*_{i+1} is computed proportionally
609 to the distance between the water table and the bottom and top depths of the $i+1$ layer:

$$\psi^{*}_{i+1} = \psi_{i+1} + \left(\psi_{sat} - \psi_{i+1}\right) \times min\left(1.0, max\left(0.0, \frac{z_{wtd} - d_{i+1}}{d_i - d_{i+1}}\right)\right) \quad \text{(A4)}$$

To sum up, if the water table is located below the ISBA soil column, then we have $\psi^{*}_{i+1} = \psi_{i+1}$, equation (A3) collapses into equation (A1) and the coupling of the water table with the soil column is solved using equation (A2) as in Decharme et al. (2019). If the water table reaches the soil column, all soil layers are "restored" towards saturation and weighted with the f_{wtd} fraction, as stated by equations (A3) and (A4).

APPENDIX B

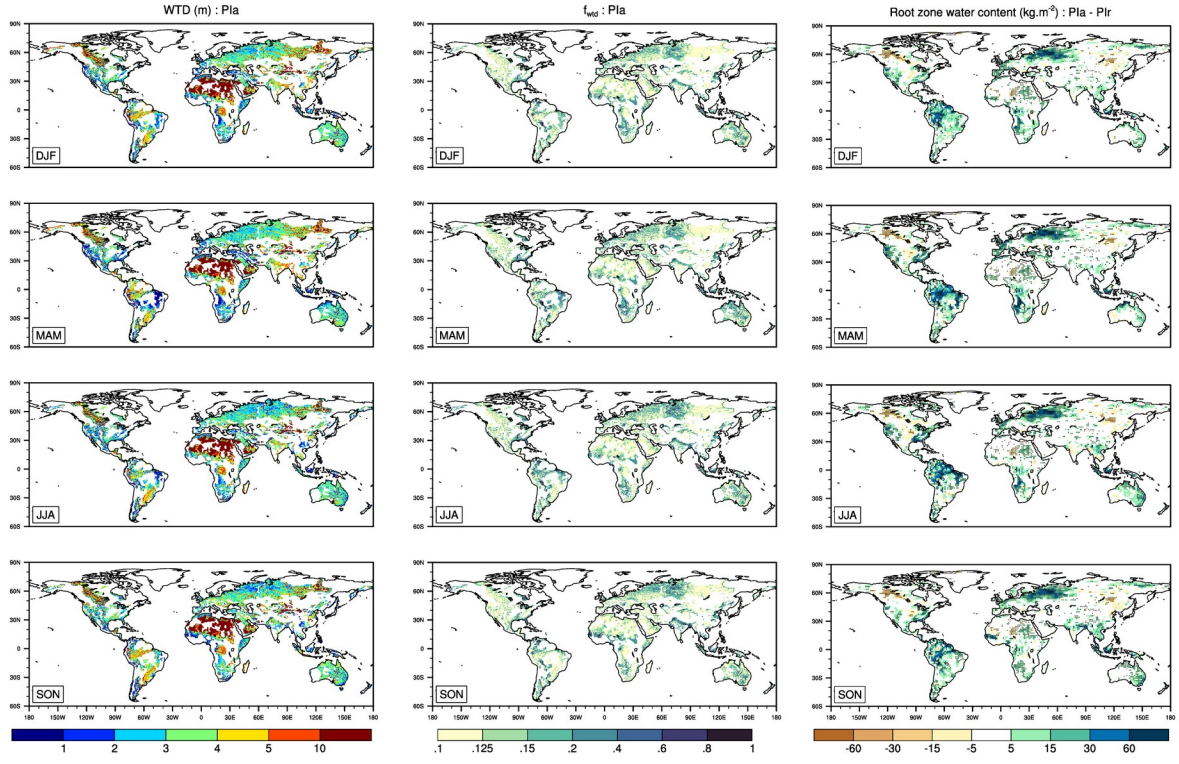

FIG. B1.

Top: seasonal mean Water Table Depth (WTD) in PIa ; middle: seasonnal mean fraction of the grid cells over which capillary rise are allowed f_{wtd} ; bottom: seasonal mean root zone water content difference with and without groundwater (PIa – PIr).

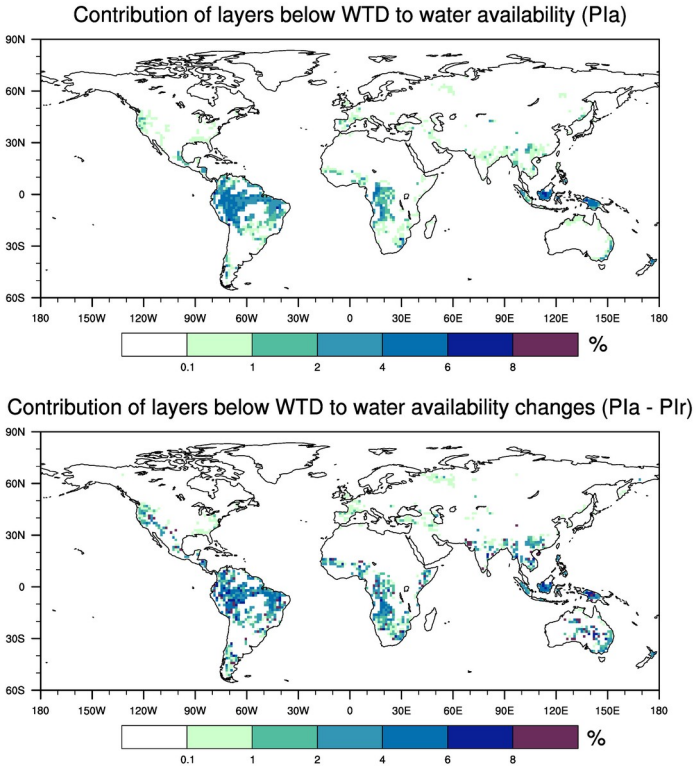

623 FIG. B2.

624 Contribution of soil layers located below the water table depth to water availability (liquid water available
625 weighted with the vertical root density profile). Top: contribution to water availability in PIa. Bottom:
626 contribution to water availability changes (PIa – PIr).

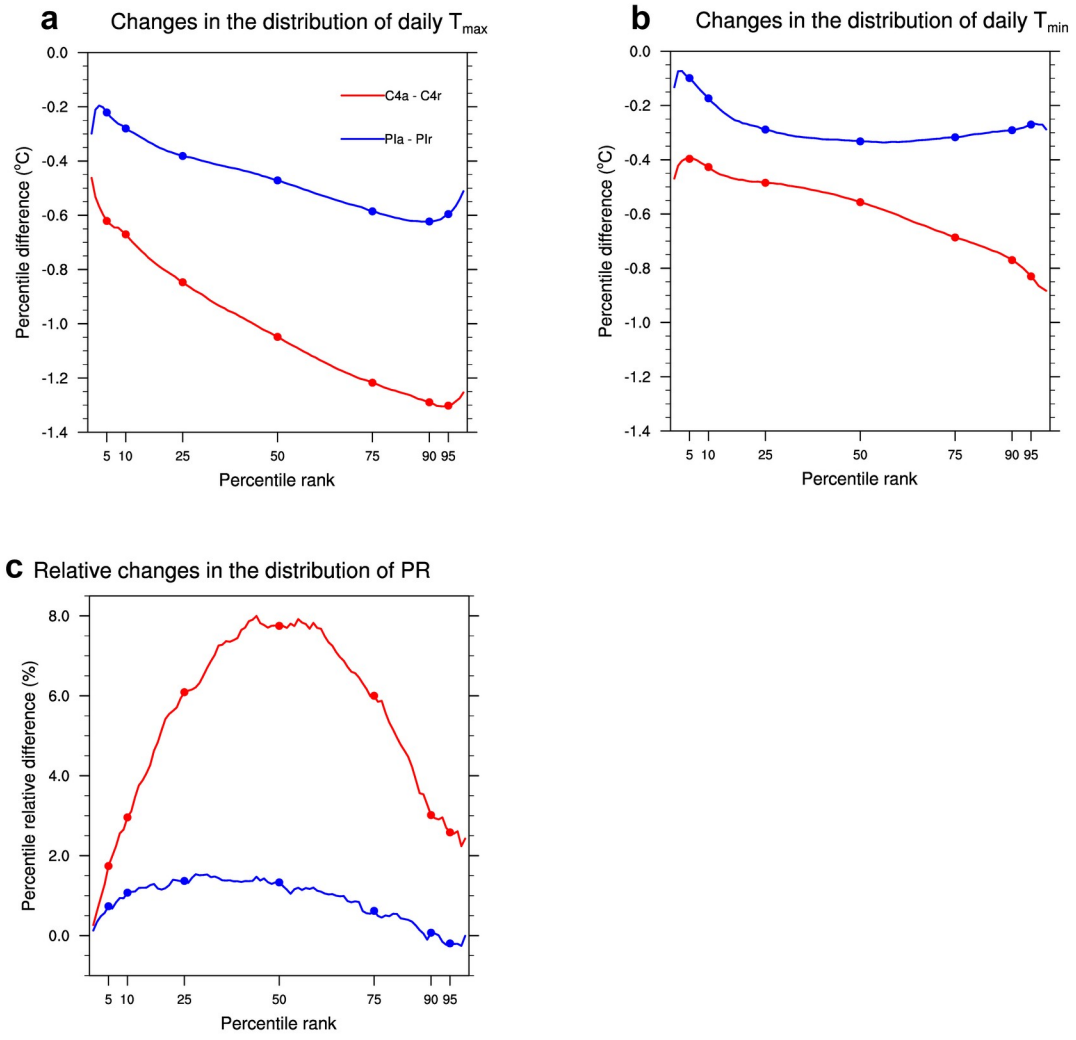

627 **FIG. B3.**

628 Differences on the summer (JJAS) percentile values (y-axis) of (a) the daily maximum 2-meter
629 temperature (°C) and (b) the daily minimum 2-meter temperature (°C). (c), relative differences (%) of the
630 summer percentile values (y-axis) of the daily precipitation rates superior to 0.1 mm.day-1 for each
631 percentile rank (x-axis). The percentiles were estimated empirically and their values were averaged over
632 the Eastern Europe box ([19°E – 60°E / 40°N – 62°N]), the blue lines represent the differences for the pre-
633 industrial simulations (PIa – PIr) and the red lines the differences in the 4xCO2 simulations (C4a-C4r), the
634 dots on the lines mark the 5%, 10%, 50% 75%, 90% and 95% percentiles.

635

636

637 REFERENCES

638 Anyah, R. O., C. P. Weaver, G. Miguez-Macho, Y. Fan and A. Robock, 2008:
639 Incorporating water table dynamics in climate modeling: 3. Simulated groundwater influence

on coupled land-atmosphere variability, *J. Geophys. Res.*, **113**, D07103, doi:10.1029/2007JD009087

Arboleda Obando, P. F., A. Ducharne, F. Cheruy, A. Jost, J. Ghattas, J. Colin and C. Nous, 2022: Influence of hillslope flow on hydroclimatic evolution under climate change, *Earth's Future*, **10**, e2021EF002613, https://doi.org/10.1029/2021EF002613

Ardilouze, C., L. Batté, B. Decharme and M. Déqué, 2019: On the Link between Summer Dry Bias over the U.S. Great Plains and Seasonal Temperature Prediction Skill in a Dynamical Forecast System. *Wea. Forecasting*, **34**, 1161–1172, https://doi.org/10.1175/WAF-D-19-0023.1

Barbeta, A. and J. Peñuelas, 2017: Relative contribution of groundwater to plant transpiration estimated with stable isotopes, *Sci Rep,* **7**, 10580, https://doi.org/10.1038/s41598-017-09643-x

Clark, M. P. and Coauthors, 2015: Improving the representation of hydrologic processes in Earth System Models, *Water Resour. Res.*, **51**, 5929-5956, https://doi.org/10.1002/2015WR017096

Danielson, J.J. and D.B. Gesch, 2011: Global multi-resolution terrain elevation data 2010 (GMTED2010): U.S. Geological Survey Open-File Report 2011-1073, 26 p. https://doi.org/10.3133/ofr20111073

Decharme, B., A. Boone, A. Delire and J. Noilhan, 2011 : Local evaluation of the Interaction between Soil Biosphere Atmosphere soil multilayer diffusion scheme using four pedotransfer functions, *J. Geophys. Res.*, **116**, D20126, https://doi.org/10.1029/2011JD016002

Decharme, B. and Coauthors, 2019: Recent changes in the ISBA-CTRIP land surface system for use in the CNRM-CM6 climate model and in global off-line hydrological applications, *Journal of Advances in Modeling Earth Systems*, **11**, 1207–1252, https://doi.org/10.1029/2018MS001545

Delire, C. and Coauthors, 2020: The global land carbon cycle simulated with ISBA-CTRIP: Improvements over the last decade, *Journal of Advances in Modeling Earth Systems*, **12**, e2019MS001886, https://doi.org/10.1029/2019MS001886

669 Dirmeyer, P. A., A. C. Schlosser, and K.L. Brubaker, 2009: Precipitation, recycling, and
670 land memory: An integrated analysis, *Journal of Hydrometeorology,* 1**0(1)**, 278-288,
671 https://doi.org/10.1175/2008JHM1016.1

672 Dirmeyer, P. A., 2011: The terrestrial segment of soil moisture–climate coupling,
673 *Geophys. Res. Lett.*, **38**, L16702, https://doi.org/10.1029/2011GL048268

674 Douville, H., J. Colin, E. Krug, J. Cattiaux and S. Thao, 2016: Midlatitude daily summer
675 temperatures reshaped by soil moisture under climate change, *Geophys. Res. Lett.*, 43, 812–
676 818, https://doi.org/10.1002/2015GL066222

677 Douville H. and Coauthors, 2020: Drivers of the enhanced decline of land near-surface
678 relative humidity to abrupt-4xCO2 in CNRM-CM6-1, *Clim Dyn,* **55,** .
679 https://doi.org/10.1007/s00382-020-05351-x

680 Dürr, H. H., M. Meybeck and S. H. Dürr, 2005: Lithologic composition of the Earth's
681 continental surfaces derived from a new digital map emphasizing riverine material transfer,
682 *Global Biogeochem. Cycles*, **19**, GB4S10, doi:10.1029/2005GB002515.

683 Evaristo, J. and J.J. McDonnell, 2017: Prevalence and magnitude of groundwater use by
684 vegetation: a global stable isotope meta-analysis, *Scientific reports,* **7**, 44110,
685 https://doi.org/10.1038/srep44110

686 Eyring, V. and Coauthors, 2016: Overview of the Coupled Model Intercomparison
687 Project Phase 6 (CMIP6) experimental design and organization, *Geosci. Model Dev.*, **9**,
688 1937–1958, https://doi.org/10.5194/gmd-9-1937-2016

689 Fan, Y., H. Li and G. Miguez-Macho, 2013: Global patterns of Groundwater Table
690 Depth, *Science*, 339 (6122), 940–943, DOI: 10.1126/science.1229881

691 Fan, Y., 2015: Groundwater in the Earth's critical zone: Relevance to large-scale patterns
692 and processes, *Water Resour. Res.*, **51**, 3052– 3069, https://doi.org/10.1002/2015WR017037

693 Fan, Y., G. Miguez-Macho, E. G. Jobbágy, R. B. Jackson, R. B. and C. Otero-Casal,
694 2017: Hydrologic regulation of plant rooting depth. *Proceedings of the National Academy of*
695 *Sciences*, *114*(40), 10572-10577, https://doi.org/10.1073/pnas.1712381114

696 Fan, Y. and Coauthors, 2019: Hillslope hydrology in global change research and Earth
697 system modeling, *Water Resources Research*, **55**, 1737–1772,
698 https://doi.org/10.1029/2018WR023903

699 Ferguson, I. M. and R. M. Maxwell, 2010: Role of groundwater in watershed response
700 and land surface feedbacks under climate change, *Water Resour. Res.*, **46**, W00F02,
701 https://doi.org/10.1029/2009WR008616

702 Fischer, E. M., S. I. Seneviratne, P. L. Vidale, D. Lüthi, and C. Schär, 2007: Soil
703 Moisture–Atmosphere Interactions during the 2003 European Summer Heat Wave, *J. of*
704 *Climate,* **20**, 5081-5099, https://doi.org/10.1175/JCLI4288.1

705 Forrester, M. M., R. M. Maxwell, 2020: Impact of lateral groundwater flow and
706 subsurface lower boundary conditions on atmospheric boundary layer development over
707 complex terrain, *Journal of Hydrometeorology,* **21(6)**, 1133-1160,
708 https://doi.org/10.1175/JHM-D-19-0029.1

709 Furusho-Percot, C., K. Goergen, C. Hartick, L. Poshyvailo-Strube and S. Kollet, 2022:
710 Groundwater model impacts multiannual simulations of heat waves, *Geophys. Res. Lett.*,
711 49(10), https://doi.org/10.1029/2021GL096781

712 Giffard, P., W. Llovel, J. Jouanno, G.Morvan and B. Decharme B. 2019: Contribution of
713 the Amazon River Discharge to Regional Sea Level in the Tropical Atlantic Ocean. *Water*,
714 **11**, 2348. https://doi.org/10.3390/w11112348

715 Gleeson, T. and Coauthors, 2021: GMD perspective: The quest to improve the evaluation
716 of groundwater representation in continental- to global-scale models, *Geosci. Model Dev.*, 14,
717 7545–7571, https://doi.org/10.5194/gmd-14-7545-2021

718 Hirschi, M. and Coauthors, 2011: Observational evidence for soil-moisture impact on hot
719 extremes in southeastern Europe, *Nature Geosci.,* **4**, 17–21, https://doi.org/10.1038/ngeo1032

720 Jiang, X., G.-Y. Niu and Z.-L. Yang, 2009: Impacts of vegetation and groundwater
721 dynamics on warm season precipitation over the Central United States, *J. Geophys. Res.*, **114**,
722 D06109, https://doi.org/10.1029/2008JD010756

723 Krakauer, N. Y., H. Li and Y. Fan, 2014: Groundwater flow across spatial scales:
724 importance for climate modeling. *Environmental Research Letters*, *9*(3), 034003

725 Keune, J., F. Gasper, K. Goergen, A. Hense, P. Shrestha, M. Sulis and S. Kollet, 2016:
726 Studying the influence of groundwater representations on land surface-atmosphere feedbacks
727 during the European heat wave in 2003, *J. Geophys. Res. Atmos.,* **121**, 13,301-13,325,
728 https://doi.org/10.1002/2016JD025426

729 Koster, R.D. and Coauthors, 2006: GLACE: the global land–atmosphere coupling
730 experiment. Part I: overview. *Journal of Hydrometeorology,* **7(4)**, 590-610,
731 https://doi.org/10.1175/JHM510.1

732 Larsen, M., Christensen, J., Drews, M., M. B. Butts and J. C Refsgaard, 2016: Local
733 control on precipitation in a fully coupled climate-hydrology model, *Sci Rep,* **6**, 22927,
734 https://doi.org/10.1038/srep22927

735 Ledoux, E., G. Girard, G. de Marsily, J.-P. Villeneuve and J. Deschenes, J., 1989:
736 Spatially Distributed Modeling: Conceptual Approach, Coupling Surface Water And
737 Groundwater. Morel-Seytoux, H.J. (eds) Unsaturated Flow in Hydrologic Modeling. NATO
738 ASI Series, **275**, Springer, Dordrecht. https://doi.org/10.1007/978-94-009-2352-2_16

739 Leung, L. R., M. Huang, Y. Qian and X. Liang, 2011: Climate–soil–vegetation control on
740 groundwater table dynamics and its feedbacks in a climate model. *Climate Dynamics*, **36(1-**
741 **2)**, 57-81, https://doi.org/10.1007/s00382-010-0746-x

742 Maxwell, R. M., F. K. Chow and S. J. Kollet, 2007 : The groundwater–land-surface–
743 atmosphere connection: Soil moisture effects on the atmospheric boundary layer in fully-
744 coupled simulations. *Advances in Water Resources*, **30**, 2447-2466,
745 https://doi.org/10.1016/j.advwatres.2007.05.018

746 Maxwell, R. and S.J. Kollet, 2008: Interdependence of groundwater dynamics and land-
747 energy feedbacks under climate change, *Nature Geosci,* **1**, 665–669,
748 https://doi.org/10.1038/ngeo315

749 Maxwell, R. M. and L. E. Condon, 2016: Connections between groundwater flow and
750 transpiration partitioning, *Science,* **353(6297)**, 377–380, DOI: 10.1126/science.aaf7891812

751 Mu, M., A. J. Pitman, M. G. De Kauwe, A. M. Ukkola, and J. Ge, 2022: How do
752 groundwater dynamics influence heatwaves in southeast Australia?, *Weather and Climate*
753 *Extremes*, 37, 100479, ISSN 2212-0947, https://doi.org/10.1016/j.wace.2022.100479

754 Munier, S. and B. Decharme, 2022: River network and hydro-geomorphological
755 parameters at 1⁄12° resolution for global hydrological and climate studies, *Earth Syst. Sci.*
756 *Data*, 14, 2239–2258, https://doi.org/10.5194/essd-14-2239-2022

757 Padrón, R.S. and Coauthors, 2020: Observed changes in dry-season water availability
758 attributed to human-induced climate change, *Nat. Geosci.* 13, 477–481,
759 https://doi.org/10.1038/s41561-020-0594-1

760 Pellet V., F. Aires, F. Papa, S. Munier and B. Decharme, 2020: Long-term total water
761 storage change from a Satellite Water Cycle reconstruction over large southern Asian basins,
762 *Hydrol. Earth Syst. Sci.*, **24**, 3033–3055, https://doi.org/10.5194/hess-24-3033-2020

763 Roehrig, R. and Coauthors, 2020: The CNRM global atmosphere model ARPEGE-Climat
764 6.3: Description and evaluation, *Journal of Advances in Modeling Earth Systems*, **12**,
765 e2020MS002075, https://doi.org/10.1029/2020MS002075

766 Saint-Martin D. and Coauthors, 2021: Tracking changes in climate sensitivity in CNRM
767 climate models, *Journal of Advances in Modeling Earth Systems*, **13**, e2020MS002190,
768 https://doi.org/10.1029/2020MS002190

769 Séférian, R. and Coauthors, 2019: Evaluation of CNRM Earth-System model, CNRM-
770 ESM2-1: role of Earth system processes in present-day and future climate, *Journal of*
771 *Advances in Modeling Earth Systems*, 11, 4182-4227, https://doi.org/10.1029/2019MS001791

772 Seneviratne, S. I., T. Corti, E. L. Davin, M. Hirschi, E. B. Jaeger, I. Lehner, I., B.
773 Orlowsky and A.J. Teuling, 2010: Investigating soil moisture–climate interactions in a
774 changing climate: A review, *Earth-Science Reviews*, **99(3-4)**, 125-161,
775 https://doi.org/10.1016/j.earscirev.2010.02.004

776 Schoetter, R., J. Cattiaux and H. Douville, 2015: Changes of western European heat wave
777 characteristics projected by the CMIP5 ensemble, *Clim Dyn,* 45, 1601–1616,
778 https://doi.org/10.1007/s00382-014-2434-8

779 Taylor, K. E., D. Williamson and F. Zwiers, 2000: The sea surface temperature and sea-
780 ice concentration boundary conditions for AMIP II simulations, PCMDI Report 60, Program
781 for Climate Model Diagnosis and Intercomparison, Lawrence Livermore National
782 Laboratory, 25 pp.

783 Vergnes, J., B. Decharme, R. Alkama, E. Martin, F. Habets and H. Douville, 2012: A
784 Simple Groundwater Scheme for Hydrological and Climate Applications: Description and
785 Offline Evaluation over France, *Journal of Hydrometeorology*, **13(4)**, 1149-1171,
786 https://doi.org/10.1175/JHM-D-11-0149.1

787 Vergnes, J. P. and B. Decharme, 2012: A simple groundwater scheme in the TRIP river
788 routing model: Global off-line evaluation against GRACE terrestrial water storage estimates
789 and observed river discharges, *Hydrology and Earth System Sciences*, 16, 3889–3908,
790 https://doi.org/10.5194/hess-16-3889-2012

Vergnes, J.-P., B. Decharme and F. Habets, 2014: Introduction of groundwater capillary rises using subgrid spatial variability of topography into the ISBA land surface model, *J. Geophys. Res. Atmos.*, **119(19)**, 11065–11086, https://doi.org/10.1002/2014JD021573

Voldoire, A. and Coauthors, 2019: Evaluation of CMIP6 DECK experiments with CNRM-CM6-1, *Journal of Advances in Modeling Earth Systems*, **11**, 2177–2213, https://doi.org/10.1029/2019MS001683

Wang, F., A. Ducharne, F. Cheruy, M.-H. Lo and J.-Y. Grandpeix, 2018: Impact of a shallow groundwater table on the global water cycle in the IPSL land–atmosphere coupled model, *Clim Dyn* **50**, 3505–3522, https://doi.org/10.1007/s00382-017-3820-9

Wilks, D. S., 2016: "The stippling shows statistically significant grid points": How research results are routinely overstated and overinterpreted, and what to do about it, *Bull. Amer. Meteor. Soc.*, 97(12), 2263–2273, https://doi.org/10.1175/BAMS-D-15-00267.1